Journal of Applied Polymer Science

Effective incorporation of TiO_2 nanoparticles into polyamide thin-film composite membranes

Seong-Joong Kim,[1,2] Pyung-Soo Lee,[1] Saira Bano,[1,2] You-In Park,[1,2] Seung-Eun Nam,[1] Kew-Ho Lee[1,2]

[1]Advanced Materials Division, Center for Membranes, Korea Research Institute of Chemical Technology, Yuseong-Gu Daejeon 305-606, Republic of Korea

[2]University of Science and Technology, Yuseong-Gu Daejeon 305-350, Republic of Korea

Correspondence to: K.-H. Lee (E-mail: khlee@krict.re.kr)

ABSTRACT: The effectiveness of TiO_2 nanoparticles in improving the performance of polyamide (PA) thin-film composite (TFC) membranes has been investigated. PA TFC membranes were prepared by interfacial polymerization with *m*-phenylenediamine (MPD) and 1,3,5-benzene tricarbonyl trichloride (TMC) where TiO_2 particles were added during and after interfacial polymerization. To distribute the TiO_2 nanoparticles uniformly in the PA films, colloidally stable TiO_2 sols were synthesized and added to the aqueous MPD solution rather than to an organic TMC solution. Through the use of different incorporation methods, TiO_2 particles were located on the top surface, in PA film layer, and in both positions. In the case of dense PA layers, the hydrophilicity of the membranes was significantly improved due to the presence of TiO_2 particles, resulting in an increased water flux. On the other hand, the enhancement of water flux was less significant when TiO_2 particles were incorporated into a loose PA film that was prepared with additives. In addition, a BSA fouling test confirmed that TiO_2 nanoparticles effectively improve the antifouling properties of the membranes for both dense and loose PA films. This effect is possibly due to increased hydrophilicity, covering of the fouling space, and a reduction in surface roughness. © 2016 Wiley Periodicals, Inc. J. Appl. Polym. Sci. **2016**, *133*, 43383.

KEYWORDS: coatings; hydrophilic polymers; membranes; polyamides

Received 11 October 2015; accepted 22 December 2015

DOI: 10.1002/app.43383

INTRODUCTION

For several decades, thin-film composite (TFC) membranes prepared by interfacial polymerization have been developed for use in reverse osmosis (RO) and nanofiltration (NF) which have been useful techniques for uses in drinking water production and desalination of sea water.[1–3] TFC membranes typically consist of ultra-thin active layers and a porous support layer. As part of efforts to maximize the performance of TFC membranes, both layers have been carefully chosen and modified, which has led to an improvement in their separation performances.[4,5] However, further improvements in the performance of TFC membranes in terms of permeability, rejection, antifouling, and chlorine resistance are still required for industrial implementation.[6–11] The following approaches regarding the enhancement of membrane performance have been suggested: developing the composite membrane using an ultra-thin layer, increasing the surface area of the active layer, introducing a composite matrix membrane containing an organic–inorganic hybrid system, and pretreatment of the surface. Among these, the novel organic–inorganic hybrid membrane combines the traditional benefits of membrane polymers with the unique properties of inorganic nanomaterials.[12] These membranes can be prepared either by direct deposition of inorganic nanomaterials onto the membrane surface or by their incorporation into the thin film during interfacial polymerization.[13] Recently, a variety of inorganic materials such as SiO_2, TiO_2, zeolite, metal oxide nanoparticles, graphene, and carbon nanotubes have been studied for use in the organic–inorganic hybrid TFC membrane.[14–17]

TiO_2 nanoparticles have a hydrophilic surface and good chemical and physical stability along with their excellent photocatalytic properties.[18,19] These features render TiO_2 nanoparticles as promising nanomaterials for organic–inorganic hybrid TFC membranes. Kwak *et al.* and Kim *et al.* studied an organic–inorganic hybrid polyamide (PA) membrane that was prepared by dipping the support membrane into a positively charged TiO_2 sol. The TiO_2 nanoparticles interacted with the PA on the membrane surface in a self-assembly interaction that originated from coordination and hydrogen bonding with carboxyl groups (-COOH). The resulting TiO_2/PA membrane exhibited a higher permeability and a new type of antibiofouling characteristic.[20–22] Madaeni and Ghaemi prepared a self-cleaning membrane using TiO_2 as a cleaning agent. In their study, TiO_2 particles were coated on a polyvinyl alcohol surface using a dipping method.[23]

Table I. Details of PA TFC Membranes Containing TiO_2

Sample	TiO_2 sol (wt %) (impregnation)	TiO_2 sol (h) (deposition)	Additives (wt %)
M0	-	-	-
M1	1-10	-	-
M2	-	1	-
M3	1-10	1	-
A0	-	-	TBP (0.6), TEA (3), CSA (3), EHD (0.2), DMSO (1.0)
A1	10	-	TBP (0.6), TEA (3), CSA (3), EHD (0.2), DMSO (1.0)
A2	-	1	TBP (0.6), TEA (3), CSA (3), EHD (0.2), DMSO (1.0)
A3	10	1	TBP (0.6), TEA (3), CSA (3), EHD (0.2), DMSO (1.0)

PA TFC membranes are generally prepared through interfacial polymerization of *m*-phenylenediamine (MPD) and 1,3,5-benzene tricarbonyl trichloride (TMC), where these are dissolved in aqueous (MPD) and organic (TMC) solutions, respectively. A porous polymer films is initially soaked in an aqueous solution, and then the excess is removed by roller. By contacting the film with the organic solution, interfacial polymerization proceeds on its surface. For a TiO_2/PA hybrid membrane, some researchers prefer to add TiO_2 nanoparticles to the organic solution.[24] This approach exposes more TiO_2 nanoparticles on the film surface, which is expected to enhance membrane performance. However, TiO_2 nanoparticles are not readily dispersed into the organic solution due to their hydrophilicity. Thus, the distribution of TiO_2 nanoparticles becomes low on the surface, possibly reducing the efficiency of TiO_2 nanoparticles as hydrophilic media.

We studied PA TFC membranes for uses in high flux RO membranes using TiO_2 nanoparticles, which were added not to an organic solution but instead to an aqueous solution containing MPD. We expected the TiO_2 nanoparticles to exhibit improved dispersion during interfacial polymerization although these would be less exposed on the surface. To further improve TiO_2 nanoparticle dispersion, a colloidally stable TiO_2 sol was synthesized by the sol–gel method, and this was directly added to the aqueous solution. The TFC membranes were fabricated both by varying the amount of TiO_2 nanoparticles and by changing the incorporation methods. The resulting membranes were evaluated in terms of their water flux, salt rejection, and antifouling properties. In addition, the incorporation of TiO_2 into loose TFC membranes that were prepared with additives was also conducted, and the performances of these membranes were characterized. Finally, the efficiency of TiO_2 nanoparticles in enhancing the performance of the membranes, with reference to the physical morphologies of the PA films, was discussed.

EXPERIMENTAL

TiO_2 Sol Synthesis

TiO_2 sol was synthesized using the sol–gel method. 29.58 mL titanium tetraisopropoxide (TIP, Aldrich) was added dropwise to the water/ethanol mixture (water:200 mL, ethanol:10 mL), and the TIP-added mixed solution was placed in an oil bath (90 °C) for 30 min, followed by vigorous stirring at room temperature for 1 h. After adding an additional 2.66 mL of HCl for peptization into the mixed solution, this was further reacted through vigorous stirring for 2 h without sealing, to remove the propanol from the solution. About 200 mL of deionized (DI) water was then added to the mixed solution, and this was then left to react at 90 °C for 18 h.[25] After the reaction and reflux of the mixed solution, a milky and opaque TiO_2 sol was obtained.

Interfacial Polymerization of PA Membrane

The PA membrane was prepared on a flat-sheet commercial polysulfone (PSF) ultrafiltration (UF) support supplied by Woongjin Chemical in Korea as described in the literature.[26] To prepare to the amine aqueous solution, the following additives were added to the DI water as a solvent: MPD (Aldrich) (2–3 wt %), triethylamine (TEA, Aldrich), D(+)−10-camphorsulfonic acid (CSA, Aldrich), 2-ethyl-1,3-hexanediol (EHD, Aldrich), and dimethyl sulfoxide (DMSO, Aldrich). The solution was then vigorously stirred for 30 min at room temperature. The transparent solution was obtained by dissolving 0.1 wt % TMC (Aldrich) and 0.6 wt % tributyl phosphate (TBP, Aldrich) in I-sol C (SK chemicals) organic solvent, and vigorously stirring for 30 min at room temperature. The PSF support was immersed in the MPD aqueous solution for 2 min, then passed through a rubber roller to remove the excess MPD aqueous solution on the PSF surface, and then dried for 1 min at room temperature. For the interfacial polymerization of the PA between the amine and acyl halide, the dried membrane was immersed in the TMC organic solution for 1 min. After annealing the membrane for 10 min at 60 °C, the PA membrane was finally rinsed with 2000 ppm K_2CO_3 aqueous solution for 2 min.

The PA TFC membranes with TiO_2 were prepared by an impregnation and deposition method. The impregnation method is a process by which TiO_2 nanoparticles are impregnated on the inside of the PA membrane active layer by adding TiO_2 sol (1–10 wt %) to the MPD aqueous solution during the interfacial polymerization process. The deposition was accomplished by immersing the PA membrane in the TiO_2 sol for 1 h after the interfacial polymerization process. Furthermore, the impregnation and deposition of TiO_2 nanoparticles were used simultaneously in the preparation of the TiO_2/PA membranes. The preparation conditions for the TiO_2/PA membranes are summarized in Table I.

Evaluation of Permeation Performance and the Fouling Test

Measurement of water flux and salt rejection was conducted using a 2000-ppm NaCl solution at a temperature of 25 °C and a pressure of 225 psi, with a flow rate of 3 L/min.[26,27] The water flux was calculated by measuring the volume of permeated water in units of L/m^{2}h, and the salt rejection was determined by the difference in conductivity between the permeate side and feed side using a conductivity meter.

$$\text{Rejection } (\%) = \left(1 - \left(\frac{C_p}{C_f}\right)\right) \times 100$$

C_p and C_f are the conductivity of the permeate side and feed sides, respectively. BSA (200 ppm) was used as a model foulant to evaluate the antifouling property of the membrane under the same conditions as the permeation measurement.[28–30]

Sample Characterization

The X-ray diffraction patterns (XRD) of the TiO_2 powder (TiO_2 sol was dried at 40 °C for 2 days) were taken using a Rigaku D/Max-2200V diffractometer attached to a Cu tube and graphite monochromator at 40 kV. Transmission electron microscopy (TEM, TECNAI G2 T-20S) was used to determine the TiO_2 nanoparticles sizes. Scanning electron microscope (SEM, XL30S, PHILIPS) imaging was performed to observe the surface morphology of the TiO_2/PA membrane, and an atomic force microscope (AFM, Nanoscope IV, Digital Instruments) was used to characterize the surface roughness. The distribution of TiO_2 nanoparticles on the surface of the PA membrane was confirmed through energy dispersive X-ray spectroscopy (EDS, Bruker Quantax 200). Attenuated total reflectance Fourier transform infrared spectroscopy (ATR-FTIR, Bruker ALPHA-P FTIR spectrometer) was used to detect the presence of the functional group on the TiO_2-coated and impregnated PA membrane. The hydrophilicity of the TiO_2/PA membrane was measured at various parts of the surfaces by contact angle measurement (CA SEO 300A). An image was taken as soon as a droplet of pure water was delivered onto the PA membrane. To ensure the reliability of the contact angle measurements, an average value was chosen for the final result after performing the measurement with the liquid drop in five different positions.

RESULTS AND DISCUSSION

Properties of TiO_2 Nanoparticles

The TEM image in Figure 1(a) shows TiO_2 nanoparticles from the synthesized TiO_2 sol dried at 40 °C for 2 days, resulting in a wormhole-like meso-structure. From the image of the separated TiO_2 particle in Figure 1(a), the particle size is taken to be approximately 7 nm. Most of the TiO_2 nanoparticles were aggregated and adjoined one another. Also, a peak area of 25.26° [101] was adopted to calculate the nanoparticle size in the XRD pattern [Figure 1(b)]. Using the Scherrer equation ($\tau = k\lambda/\beta\cos\theta$), the mean size τ is determined by the shape factor k, the X-ray wavelength λ, the full width at half maximum (FWHM, β) and the Bragg angle θ. The TiO_2 nanoparticles sizes measured in this way were between 7 and 8 nm. The XRD peak of the synthesized particles is very similar that of to KCT-2 TiO_2 that was developed previously.[25] The majority of the TiO_2 peaks showed the anatase phase, which is known for its outstanding photocatalytic properties and hydrophilicity.[24] A minor diffraction peak originating from the brookite crystal phase also appeared.

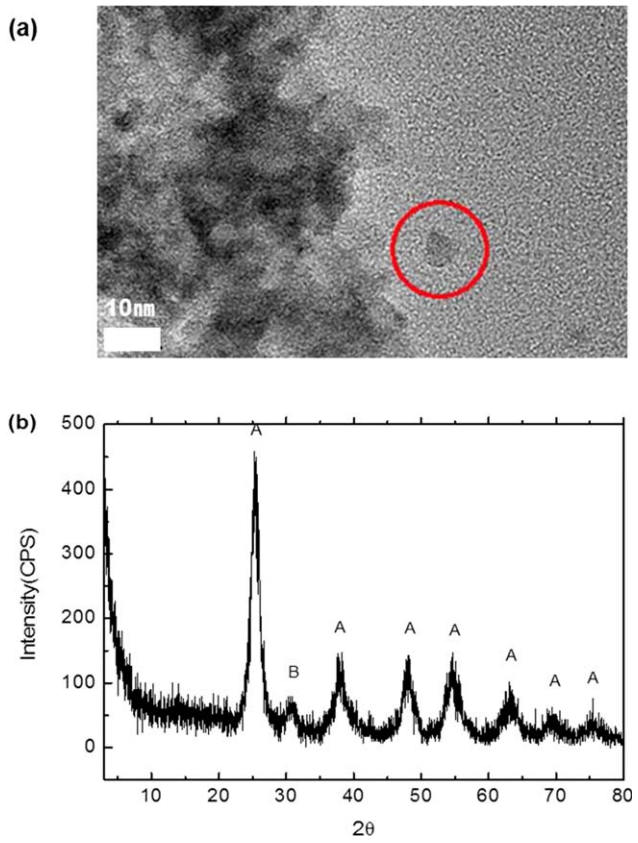

Figure 1. (a) TEM image and (b) XRD pattern of synthesized TiO_2 nanoparticles. [Color figure can be viewed in the online issue, which is available at wileyonlinelibrary.com.]

Characteristics of the PSF Support and PA TFC Membrane

Figure 2 shows SEM images of the surface of the PSF support before interfacial polymerization, and the PA layer that was later formed on it. As shown in Figure 2, the PSF support consists of a number of pores, and these were then completely blocked by the PA layer after interfacial polymerization. It is known that the PA TFC membrane is likely to be composed of pores of several Å in size, which are invisible in the SEM image. The surface of the PSF support appears to be smooth (low roughness) while the surface of the PA membrane shows a rough ridge and valley structure. Table II shows the water flux and salt rejection of the PSF supports and the PA membranes on the supports. As shown in Table II, the PSF supports exhibited high water flux and low salt rejection because of the presence of nonselective pores, as shown in Figure 2. On the other hand, the PA membranes prepared by the interfacial polymerization of MPD and TMC, exhibited a salt rejection higher than 94% as shown in Table II. The water flux and salt rejection of the PSF support were 824.9 L/m^{2}h and 6.82% respectively, at a pressure of 225 psi. The flux of the PA membrane that was prepared by interfacial polymerization was significantly decreased to a value of 0.83 L/m^{2}h. The thin and dense PA layers (thickness of 100–

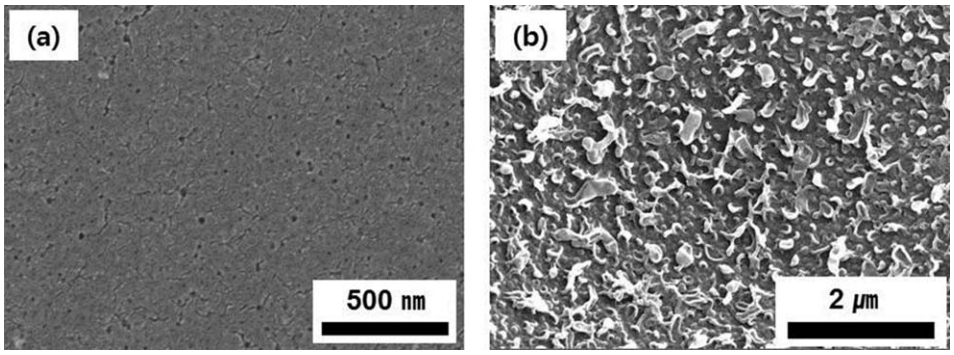

Figure 2. FE-SEM images of (a) PSF support and (b) PA membrane.

200 nm) on the PSF support were coated through the interfacial polymerization of MPD (amine) and TMC (acyl halide), which caused a significant reduction in the flux together with an increase of rejection.[31] This indicates that it is desirable to enhance the flux of the PA membrane. Several methods such as modification through the use of additives and postprocessing have been proposed to this end.

TiO_2 Effect on a Dense PA TFC Membrane

To improve the water flux of the PA membrane, we incorporated TiO_2 nanoparticles into the membrane by impregnation (by adding TiO_2 into the MPD solution), deposition (by dip-coating), and both impregnation and deposition, as described in the experimental section. Figure 3 shows SEM images of the PA membrane after TiO_2 incorporation. As shown in Figure 3, the PA membrane displays noticeably different distributions of TiO_2 on the membrane surfaces, according to the incorporation method used. In the case of M0 that was prepared with only MPD and TMC and without TiO_2 nanoparticles, as shown in Figure 3(a), a ridge and valley structure was visible on the surface of the PA layer. The TiO_2 was not visible in the SEM image [Figure 3(b)] for M1, which was prepared by impregnation. However, the EDS mapping analysis provided in the inset of Figure 3(b) indicated the presence of TiO_2 inside the membrane, and also confirmed the presence of a large amount of impregnated nanoparticles throughout the membrane with a uniform distribution as indicated by red dots. In our study, a high dispersion of nanoparticles is believed to originate from the approach of adding the hydrophilic TiO_2 sol directly into an aqueous solution, and not into a TMC organic solution. If TiO_2 nanoparticles are added to an organic solution, the dispersion of the powder will be low due to the aggregation and precipitation of particles in the organic solution. The PA layer of M2 that had been immersed in TiO_2 sol for 1 h was wholly covered with the deposited nanoparticles [Figure 3(c)]. As shown in Figure 3(d), among the samples, the largest amount of the TiO_2 nanoparticles was present on the membrane surface of M3. This is because the impregnated TiO_2 in the PA layer increased the affinity for adsorption of nanoparticles during immersion coating.

Figure 4 shows the contact angles of the TFC PA membrane and ATR spectra before and after the addition of TiO_2. The contact angle results indicate that M2 (68.11°) exhibited a higher hydrophilicity than M0 (79.08°) and M1 (78.12°). The lowest contact angle was observed in M3. The contact angle of M3 (31.58°) indicates that this sample exhibited a more hydrophilic surface due to a greater amount of TiO_2 nanoparticles deposited on the M3 surface compared to M0, M1, or M2. At the moment water was dropped onto the surface of M3, it spread over a wide area because of the ultra-hydrophilic property of the TiO_2, that was distributed over the surface.[32] The presence of TiO_2 on the PA layer was further confirmed by the ATR-IR spectra, shown in Figure 4(e). The peak (400–1000 cm^{-1}) of M3 that was related to TiO_2 bonds was significantly lower and wider than the peak of the pure PA membrane (M0).[33] Moreover, the absorption peak of the hydroxyl group (3000–3500 cm^{-1}) also became stronger due to the surface hydroxyl group of TiO_2 from M3. Thus, it can be concluded that M3 exhibited a more hydrophilic surface and higher TiO_2 loading than the other samples.

Table III indicates that the flux was dependent on the amounts of TiO_2 and their positions in the PA membrane. A positive correlation exists here: increasing the amount of TiO_2 sol that was added to the amine aqueous solution led to an increase in the flux. M0 exhibited a very low flux of approximately 0.83 L/m^2h while M1, M2, and M3 showed enhanced water flux with increasing weight percent of TiO_2. Among these samples, the flux of M3 (22.84 L/m^2h) appeared to be the highest, twice those of M1 (9.54 L/m^2h) and M2 (11.88 L/m^2h). It is understood that M3 was able to bear a greater amount of TiO_2 particles because the nanoparticles were placed both on the surface and inside the PA layer.

It is of note that the salt rejection of the prepared membranes exhibited a different behavior. Comparing M0 and M1, there was almost no change in salt rejection while the water flux increased as the weight of TiO_2 increased. Similar trends were observed for M3 (3%) and M3 (5%). This indicates that TiO_2 worked effectively to enhance membrane performance. A slight reduction in salt rejection for M3 (10%) is thought to be associated with defects created at interface of inorganic materials and polymer matrix because of high loading. On the other hand, noticeable reductions were observed for M2 and M3 (1%). The salt rejections were initially expected to remain the

Table II. Performance of the PSF Support and PA Membrane (2000 ppm NaCl Solution, 225 psi)

	PSF support	PA membrane (M0)
Flux (L/m^2h)	824.91	0.83
Rejection (%)	6.82	94.83

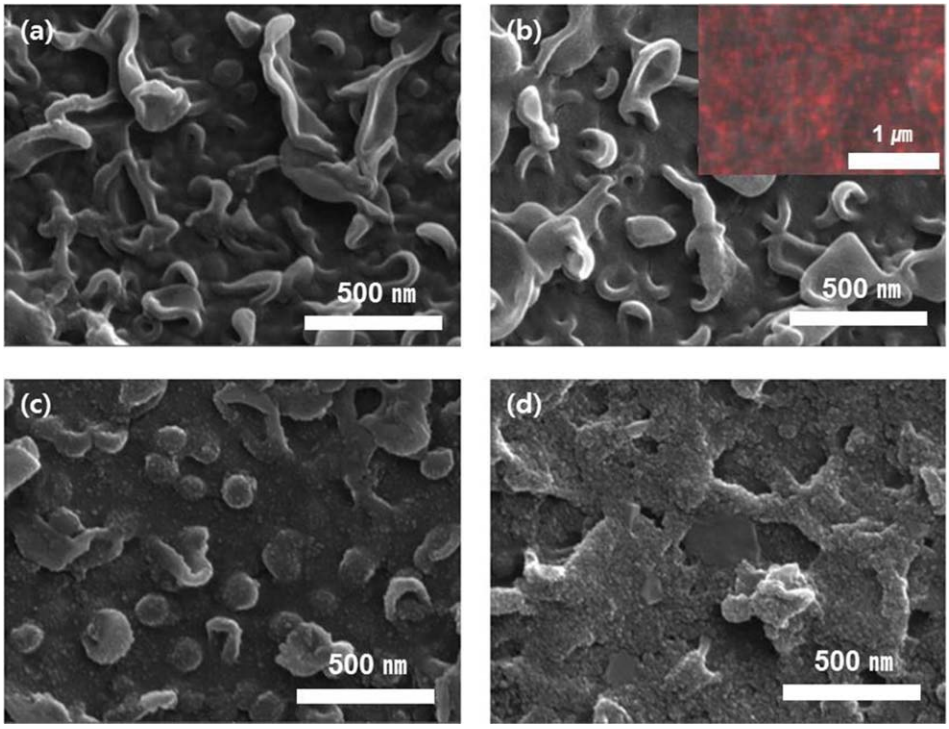

Figure 3. FE-SEM images of the surface morphologies of TiO_2-impregnated or/and deposited PA membranes. (a) M0: PA membrane (no TiO_2), (b) M1 (1 wt %): TiO_2-impregnated PA membrane and EDS mapping image, (c) M2: TiO_2-deposited PA membrane, and (d) M3 (1 wt %): TiO_2-impregnated and deposited PA membrane). [Color figure can be viewed in the online issue, which is available at wileyonlinelibrary.com.]

same or to increase for both samples, since the addition of TiO_2 proved to increase the water flux while maintaining salt rejection. We postulated that chlorine included in the TiO_2 sol led to a reduction in salt rejection by degrading the PA membrane. As described in the Experimental section, HCl was selected as a catalyst for TiO_2 hydrolysis and condensation, and the resulting TiO_2 sol was directly used for membrane fabrication and coating without further purification. Thus, chlorine ions were present during interfacial polymerization and immersion for the TiO_2 coating, and their concentration could have been greater than several thousand ppm. Thus, chlorine in TiO_2 sol would degrade the membranes and create nonselective regions on the PA layer. In addition, the salt rejections of M3 (3%) and M3 (5%) were recovered to values similar to those of M0 and M1 as shown in Table III. Thus, it is likely that TiO_2 can exhibit a certain amount of chlorine tolerance by embedding on the surface of the PA layer. We may speculate that a strong interaction between the TiO_2 nanoparticles and the polymer happens as a result of coordination or hydrogen bonding with COOH groups and might contribute to the observed enhancement in chlorine tolerance. However, this still requires further clarification and so further investigations haves been formed.

TiO_2 Effect on a Loose PA TFC Membrane Prepared with Additives

High-flux membranes were prepared by adding additives such as TEA, CSA, EHD, DMSO and TBP. It has been reported that these additives improve the water flux of membranes by making these more porous and hydrophilic.[26] The performance of the PA TFC membrane that was prepared with additives is summarized in Table IV. It is shown that additives increased the water flux of the membranes where A0 exhibited a flux of 80.29 L/m^{2}h and a salt rejection of 87.76%. A0 exhibited a higher flux than M0 because of an additive effect that considerably changed the morphology of the PA layers, shown in Figure 5(a). The flux of A1, prepared with 10 wt % TiO_2 sol-added to an amine aqueous solution, was slightly higher than that of A0 but with a reduced salt rejection. Thus, TiO_2 nanoparticles did not produce a corresponding increase in the water flux of A1, compared with that of M1. In the case of A2, which was dipped in the TiO_2 sol for 1 h, the flux became even lower at a value of 66.74 L/m^{2}h. The lowest flux was exhibited by A3, which underwent both impregnation and deposition of TiO_2 nanoparticles, at only 55.88 L/m^{2}h. As shown in Figure 5(a,b), the high fluxes of A0 and A1 originated from the porous morphology of the PA film. On the other hand, in the cases of A2 and A3, the TiO_2 particles were positioned in the cavities and caused a narrowing of the passage of water molecules, as shown in Figure 5(c,d), which is shown to decrease the water flux in spite of the increase in hydrophilicity.

Figure 6 exhibit AFM images of M0, M3, A0, and A3 as well as contact angles of A0 and A3. As compared with the root mean squared roughness (R_{rms} = 12.4 nm) of M0 [Figure 6(a)], the surface of A0 [Figure 6(c)] presented low roughness as 8.6 nm in R_{rms} by AFM, which corresponds to the previous study.[26] The contact angle of A0 was measured to 60.23°, that was lower than that of M0 (79.08°) as well. The low roughness would lead to decrease in the contact angles. Thus, reduction in surface roughness of A0 also played a role to improve water flux, along with their porous structures by additives. Changes in surface

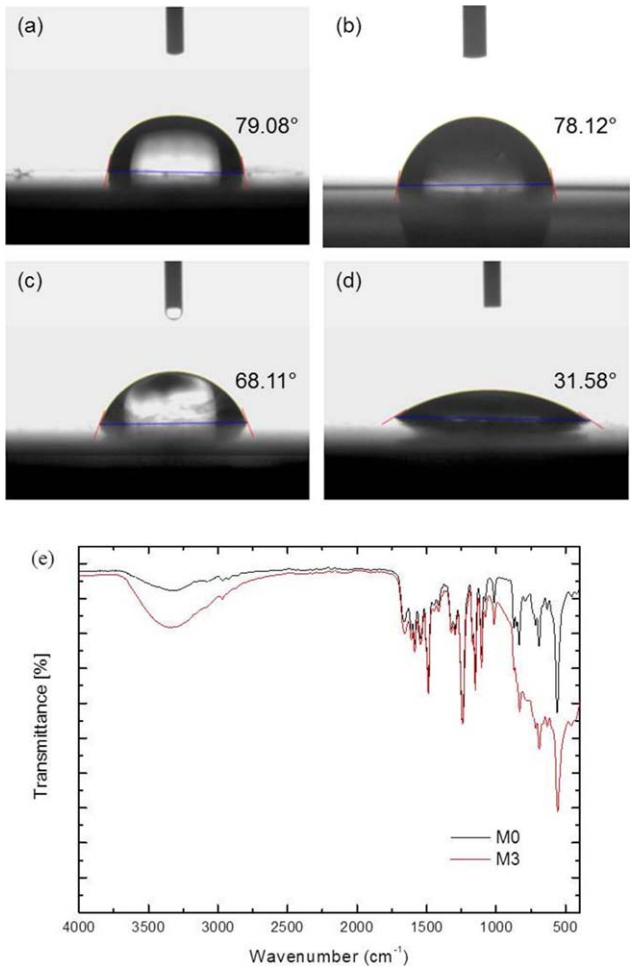

Figure 4. Contact angle of TiO_2-impregnated or/and deposited PA membranes. (a) M0: no TiO_2, (b) M1 (1 wt %): TiO_2 impregnation, (c) M2: TiO_2 deposition, (d) M3 (1 wt %): TiO_2 impregnation + deposition, and (e) ATR spectra of M0 and M3. [Color figure can be viewed in the online issue, which is available at wileyonlinelibrary.com.]

morphology resulting from TiO_2 deposition can be visualized using AFM where R_{rms} of M3 [Figure 6(b)] and A3 [Figure 6(d)] were calculated as 7.9 and 5.7 nm, which were smother than M0 and A0, respectively. TiO_2 particles placed on the PA surfaces led to reduction in their surface roughness. As shown in Figure 6(f), the contact angle of A3 was further reduced to 30.20°, which is similar to that of M3 (31.58°). However, differing from M3 enhancing the water flux, A3 exhibited a reduction in the water flux although salts rejected were improved. TiO_2 particles on A3 were likely to narrow its void spaces and eventually decreased the water permeance. Thus, the addition of TiO_2 nanoparticles into a high flux of loose PA membranes prepared with additives appeared to be less effective than in the dense PA membranes.

Antifouling Properties of PA TFC Membranes with TiO_2 Loading

Antifouling testing was conducted using a 200-ppm BSA aqueous solution, a common organic foulant employed for these tests. Figure 7 shows the fouling resistance of the resulting membranes. As shown in Figure 7, there were practically no changes in the flux among M0, M1, M2, and M3 for 6 h, whereas the other samples showed a noticeable reduction in water flux. This trend originates from a difference in the flux of the membranes and their morphologies. While water molecules selectively pass through certain membranes, other impurities are being rejected by the membranes forming cake layers on the membrane surface. This reflected the fact that the cake layers grow quicker as the water flux of a membrane increased, resulting in flux reduction because of diffusion resistance by the accumulated cake layers. Thus, it is shown that cake layers were thinner in the former samples because of low flux, but more cake was accumulated in the other samples. Furthermore, the latters exhibited more cavities on their surfaces because of the additives inserted during interfacial polymerization. These spaces may provide more possibilities for foulants to remain on the membrane surface during water permeation.

The antifouling effect of TiO_2 nanoparticles can be visualized through a comparison of A0, A1, A2, and A3. It may be seen from Figure 7 that resistance to fouling could be improved by the addition of TiO_2 nanoparticles. In particular, this appeared to be effective when TiO_2 particles were present on the surface rather than in the PA layer. A2 exhibited higher antifouling resistance than A1. A3 exhibited the maximum resistance among the high flux PA membranes because of the presence of TiO_2 both on the surface and in the PA film. From these results, it can be concluded TiO_2 particles can enhance resistance to

Table III. Performance of PA TFC Membranes According to TiO_2 Sol Concentration

		M1					M3			
	M0	1%	3%	5%	10%	M2	1%	3%	5%	10%
Flux (L/m^{2}h)	0.83	2.36	3.40	5.58	9.54	11.88	13.99	16.25	21.69	22.84
Rejection (%)	94.83	93.38	94.13	95.57	94.97	85.64	85.19	94.95	94.33	91.42

Table IV. Performance of PA TFC Membranes That Were Prepared with Additives and TiO_2 Nanoparticles

	A0 (no TiO_2)	A1 (impregnation)	A2 (deposition)	A3 (impregnation+deposition)
Flux (L/m^{2}h)	80.29	84.10	66.74	55.88
Rejection (%)	87.76	85.39	91.70	93.29

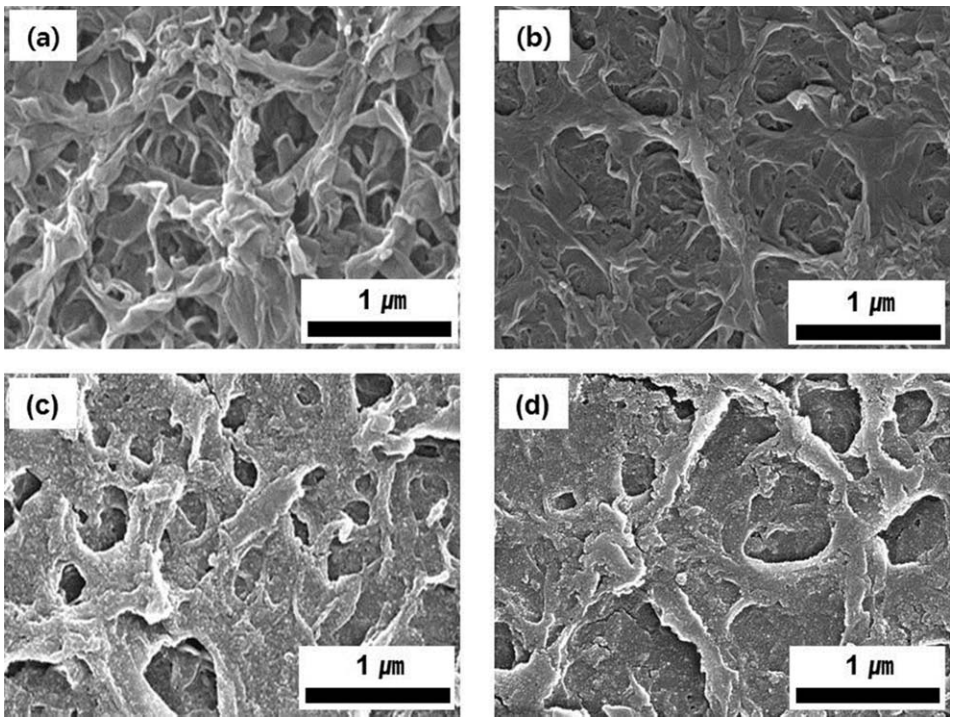

Figure 5. FE-SEM images of the surface morphologies of PA membranes that were prepared with additives and TiO_2 nanoparticles. (a) A0: PA membrane (no TiO_2), (b) A1: TiO_2-impregnated PA membrane, (c) A2: TiO_2-deposited PA membrane, and (d) A3: TiO_2-impregnated and deposited PA membrane).

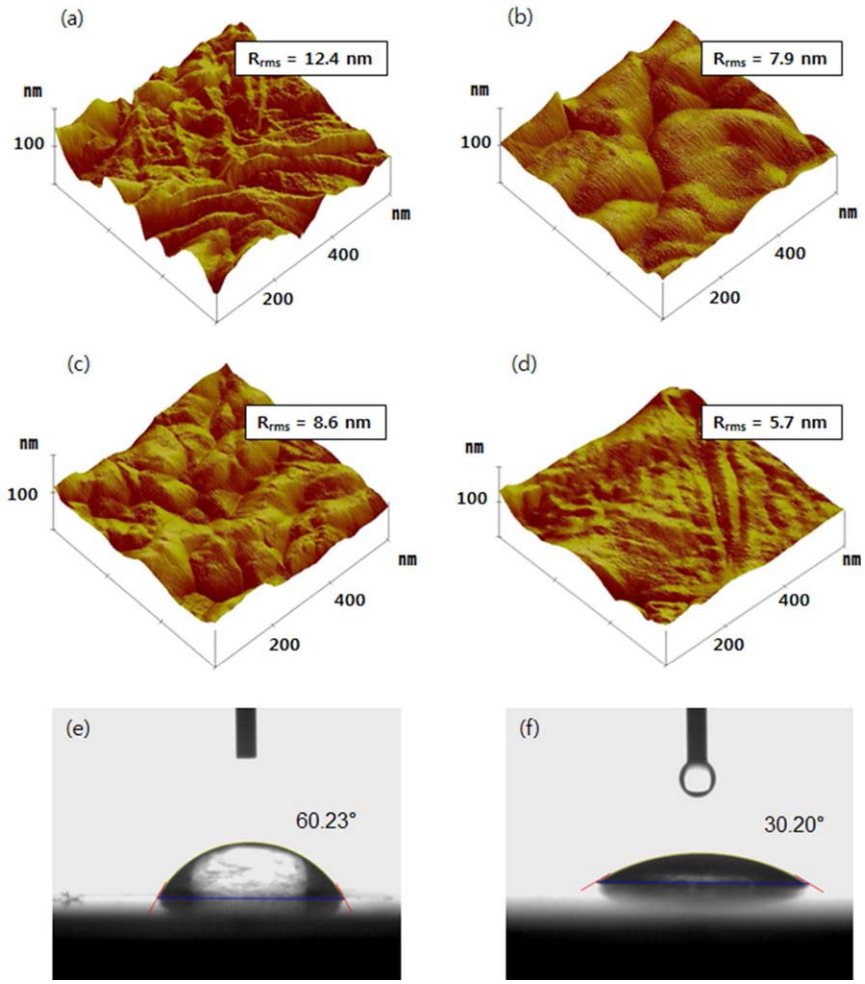

Figure 6. Surface roughness of (a) PA membrane (M0) prepared without TiO_2 nanoparticles, (b) TiO_2/PA membrane (M3) produced using the impregnation and deposition method with TiO_2 nanoparticles, (c) PA membrane (A0) prepared only with additives, (d) TiO_2/PA membrane (A3) produced using the impregnation and deposition method with both additives and TiO_2 nanoparticles, and (e) and (f) contact angles of A0 and A3, respectively. [Color figure can be viewed in the online issue, which is available at wileyonlinelibrary.com.]

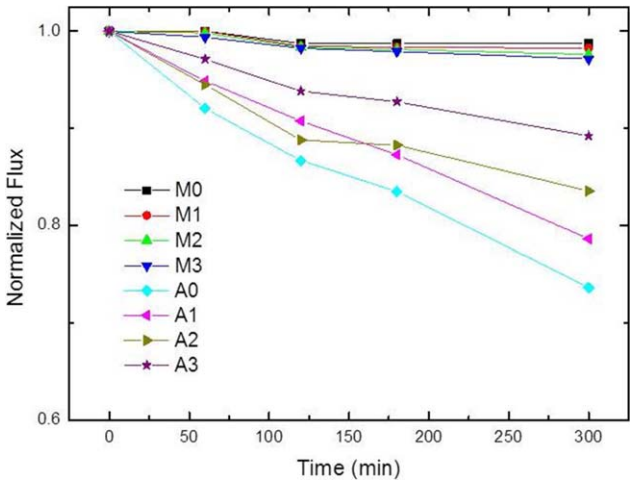

Figure 7. Fouling test (200 ppm BSA aqueous solution) for TiO_2/PA membranes prepared with additives. [Color figure can be viewed in the online issue, which is available at wileyonlinelibrary.com.]

organic foulants by providing hydrophilic properties to the PA layer.

CONCLUSIONS

TiO_2 nanoparticles have been incorporated into PA TFC membranes, by both impregnation and deposition. We prepared colloidally stable TiO_2 sols and added these to an aqueous MPD solution to enhance the dispersion of TiO_2 particles on a PA film. It is clear that the presence of the TiO_2 particles led to an increase in the hydrophilicity of the PA TFC membranes, while the efficiency of TiO_2 particles appeared to differ depending on the physical structure of the PA film. For the case of dense PA films, enhancement by TiO_2 particles was significant, and the water flux was improved by 10 times. However, TiO_2 did not play such a significant role in the case of loose PA membranes that were prepared with additives. In this case, only modest changes were observed, regardless of TiO_2 loading. Thus, it can be concluded that the addition of TiO_2 particles works effectively for dense PA TFC membranes, as these exhibited great improvement in the water flux. In addition, the BSA fouling tests confirmed that the fouling problem for organisms could be mitigated by the presence of TiO_2 because of the effects of hydrophilicity, pore covering by TiO_2, and a reduction in surface roughness. The membranes proposed by this study featured extremely high water fluxes and salt rejections above 94%, which appeared rather low for desalination requiring salt rejections as high as 99.7%. Instead, these high flux membranes would potentially be used for household water purifier as well as recovery of special chemicals such as pigments and draw solutes for FO (Forward osmosis) membranes.

REFERENCES

1. Saleh, T. A.; Gupta, V. K. *Sep. Purif. Technol.* **2012**, *89*, 245.
2. Ji, J.; Mehta, M. *J. Membr. Sci.* **2001**, *192*, 41.
3. Ji, J.; Dickson, J. M.; Childs, R. F.; McCarry, B. E. *Macromolecules* **2000**, *33*, 624.
4. Prakash Rao, A.; Joshi, S. V.; Trivedi, J. J.; Devmurari, C. V.; Shah, V. J. *J. Membr. Sci.* **2003**, *211*, 13.
5. Ahmad, A. L.; Ooi, B. S. *J. Membr. Sci.* **2005**, *255*, 67.
6. Shintani, T.; Matsuyama, H.; Kurata, N. *Desalination* **2009**, *247*, 370.
7. Song, Y.; Liu, F.; Sun, B. *J. Appl. Polym. Sci.* **2005**, *95*, 1251.
8. Xu, G. R.; Wang, J. N.; Li, C. J. *Desalination* **2013**, *328*, 83.
9. Zhang, Z.; Wang, Z.; Wang, J.; Wang, S. *Desalination* **2013**, *309*, 187.
10. Violleau, D.; Essis-Tome, H.; Habarou, H.; Croue, J. P.; Pontie, M. *Desalination* **2005**, *173*, 223.
11. Son, S. H.; Jegal, J. *J. Appl. Polym. Sci.* **2011**, *120*, 1245.
12. Jeong, B. H.; Hoek, E. M. V.; Yan, Y.; Subramani, A.; Huang, X.; Hurwitz, G.; Ghosh, A. K.; Jawor, A. *J. Membr. Sci.* **2007**, *294*, 1.
13. Kang, G.; Cao, Y. *Water Res.* **2012**, *46*, 584.
14. Fathizadeh, M.; Aroujalian, A.; Raisi, A. *J. Membr. Sci.* **2011**, *375*, 88.
15. Kong, C.; koushima, A.; Kamada, T.; Shintani, T.; Kanezashi, M.; Yoshioka, T.; Tsuru, T. *J. Membr. Sci.* **2011**, *366*, 382.
16. Rajaeian, B.; Rahimpour, A.; Tade, M. O.; Liu, S. *Desalination* **2013**, *313*, 176.
17. Vinodh, R.; Sangeetha, D. *J. Appl. Polym. Sci.* **2013**, *128*, 1930.
18. Porkodi, K.; Arokiamary, S. D. *Mater. Charact.* **2007**, *58*, 495.
19. Yang, S.; Gu, J. S.; Yu, H. Y.; Zhou, J.; Li, S. F.; Wu, X. M.; Wang, L. *Sep. Purif. Technol.* **2011**, *83*, 157.
20. Kim, S. H.; Kwak, S. Y.; Sohn, B. H.; Park, T. H. *J. Membr. Sci.* **2003**, *211*, 157.
21. Kwak, S. Y.; Kim, S. H.; Kim, S. S. *Environ. Sci. Technol.* **2001**, *35*, 2388.
22. Kwak, S.-Y.; Kim, S.-H.; Kim, S.-S. Patents (**2003**).
23. Madaeni, S. S.; Ghaemi, N. *J. Membr. Sci.* **2007**, *303*, 221.
24. Lee, H. S.; Im, S. J.; Kim, J. H.; Kim, H. J.; Kim, J. P.; Min, B. R. *Desalination* **2008**, *219*, 48.
25. Lee, D. W.; Lee, K. H. *Micropor. Mesopor. Mater.* **2011**, *142*, 98.
26. Kim, I. C.; Jeong, B. R.; Kim, S. J.; Lee, K. H. *Desalination* **2013**, *308*, 111.
27. Kwon, Y. N.; Leckie, J. O. *J. Membr. Sci.* **2006**, *282*, 456.
28. Sim, L. N.; Wang, Z. J.; Gu, J.; Coster, H. G. L.; Fane, A. G. *J. Membr. Sci.* **2013**, *443*, 45.
29. Mansourpanah, Y.; Madaeni, S. S.; Rahimpour, A.; Farhadian, A.; Taheri, A. H. *J. Membr. Sci.* **2009**, *330*, 297.
30. Al-Amoudi, A.; Lovitt, R. W. *J. Membr. Sci.* **2007**, *303*, 4.
31. Kong, C.; Kanezashi, M.; Yamomoto, T.; Shintani, T.; Tsuru, T. *J. Membr. Sci.* **2010**, *362*, 76.
32. Wu, G.; Gan, S.; Cui, L.; Xu, Y. *Appl. Surf. Sci.* **2008**, *254*, 7080.
33. Seyedjamali, H.; Pirisedigh, A. *Colloid Polym. Sci.* **2011**, *289*, 15.